IEEE Access
Multidisciplinary ⋮ Rapid Review ⋮ Open Access Journal

Received June 27, 2020, accepted August 1, 2020, date of publication August 17, 2020, date of current version August 31, 2020.

Digital Object Identifier 10.1109/ACCESS.2020.3017144

Mathematical Model and Experimental Design of Nanocomposite Proximity Sensors

REZA MOHEIMANI[1,2], ABDOLREZA PASHARAVESH[1,2], MANGILAL AGARWAL[2], (Senior Member, IEEE), AND HAMID DALIR[2], (Senior Member, IEEE)

[1]School of Mechanical Engineering, Purdue University, West Lafayette, IN 47907, USA
[2]Integrated Nanosystems Development Institute, Purdue School of Engineering and Technology, IUPUI, Indianapolis, IN 46202, USA

Corresponding authors: Mangilal Agarwal (agarwal@iupui.edu) and Hamid Dalir (hdalir@iupui.edu)

This work was supported in part by the Integrated Nanotechnology Development Institute (INDI) and in part by the National Science Foundation Major Research Instrumentation Program for the FESEM under Award 1229514.

ABSTRACT A mathematical model of fringe capacitance for a nano-based proximity sensor, which takes the presence of different resistivities into account, is developed. An analytical solution obtained for a rectangular-shape sensor with applying of Gauss, Conversation of Charge and Ohm laws into Laplace's equation $\nabla^2 V(x, y, z, t) = 0$ gives the electric potential distribution by which the fringe capacitance in a 2D domain area can be calculated. The calculated capacitance evidently decreases drastically due to the fringe phenomena while object moves toward the polymeric sensor. The model also asserts that the change of capacitance is under a noticeable influence of sensor resistivity, particularly in the range of 10^3-$10^5\Omega$.m, the initial capacitance varies from 0.045pF to 0.024 pF. The fabricated flexible nanocomposite sensors, Thermoplastic Polyurethane (TPU) reinforced by 1wt.% Carbon Nanotubes (CNTs) having resistivity $10^5\Omega$.m, are capable of detecting presence of an external object in a wide range of distance and indicating remarkable correlation with the mathematical solution. Our proximity sensor fabrication is straightforward and relatively simple. An unprecedented detection range of measurement reveals promising ability of this proximity sensor in applications of motion analysis and healthcare systems.

INDEX TERMS Fringe capacitance, nanostructure composite systems, proximity sensor, Laplace's equation.

I. INTRODUCTION

The evolution of sensor engineering has made a spectacular development for years in many existing and emerging applications, including robotic technologies, human-machine interfacing, bioelectronic devices, and electronics skins [1]–[11]. Multiple flexible or stretchable sensors have been developed by Micro-electro-mechanical system (MEMS) micromachining techniques for different purposes. For instance, strain sensors can detect body motion [7], [11], [12], tactile sensors enable to monitor three-axis handling/manipulation of objects [9], [13], [14], while proximity sensors avoid any possible accident of humans and robots to unknown obstacles [2], [3], [15]. Although most measurements made in sensor industry are of a deformation-based nature, proximity distance measurement becomes an increasing prevalence in wearable electronics which need to interact with human being and environment safely. Hence, it is necessary to be able to detect the presence of the object without making contact. To benefit the contactless measurement, a couple of studies have been carried out on incorporation of proximity sensing function to the applications for other types of sensors like, tactile, pressure and strain sensors [3], [15]–[18]. Therefore, it becomes desirable to integrate proximity sensors in many electronic platforms as much as possible. Up to now, various types of proximity sensors have been manufactured in market such as ultrasonic, infrared, magnetic induction, and capacitive sensors. Among the different detection mechanisms, capacitance-based proximity sensors have been deployed more than the others thanks to their simple device design, easy readout, integration and unbiased functionality respect to different color and texture while detecting [7], [16], [19]–[22].

Technically, the mechanism of capacitive proximity sensors (CPS) is usually governed by two principles which are based on either a traditional parallel-plate capacitor or fringe capacitance (also named planar capacitive sensors).

The associate editor coordinating the review of this manuscript and approving it for publication was Ahmed Mohamed Ahmed Almradi.

Though parallel-plate proximity sensor has a straightforward mechanism and wide applications, it exhibits some major limitations, including the approaching object must be conductor, sensitivity drops drastically while the gap between two plates increases, and eventually this type is not applicable when the media of measurement is inaccessible(one plate is spinning or in the water) [23]. Recently, a large number of CPSs applying the principle of fringe capacitance have been proposed. Here, a CPS, a device that consists of two live electrodes located on either side of conductive substrate, transduces stimuli movement to capacitance signal. Furthermore, an object, which is aimed to be detected in the vicinity of the sensor, does not have to be part of the structure, and it can also be either a conductor or nonconductor [17], [21]–[26].

Lately, modeling, implementation and analysis of CPS were extensively presented on the variation of the fringe. In capacitive displacement sensing perspective, as an object approaches a CPS, the relative change in capacitance between two electrodes (mutual capacitance mode) is recorded. There are three methods for modeling of the proximity sensor: the technique of images [27], the technique of conformal map [28], and the method of solution of Laplace's equation. However, very few analyses have been examined on the latter one due to its nonlinear feature. Mostly, studies are limited to empirical formula and numerical simulation to anticipate an analytical formula for varied geometry of proximity sensors. Noltingk [29] firstly reported CPS functioning based on the fringe effect. They theoretically analyzed two quite large types of sensing structure, constructed in the ring-shaped and rectangular electrode. Chuang *et al.* [30] presented a fringe capacitance formula of microstructures with derivation of an empirical formula for the capacitance. The empirical formula is obtained by using curve fitting on numerous ANSYS numerical simulation within dimension ranges of plate and ground. To detect damage location in power system cables, PCSs with an interdigitated structure showed the great potential for nondestructive monitoring of the insulation status [31]. Due to the inherent difficulty in developing exact analytical formulas for such a complicated geometry, authors suggested an empirical equation based on Ansoft Maxwell simulation and experimental measurements [31].

Although empirical models describing planar capacitive sensor exist, they do not provide actual insight into the interaction of the electric field with the moving object nor do they explain the actual interaction of different parameters in the sensing mechanism. With this in mind, to explore the fringe effect of parasitic capacitance for nanoscale metal–oxide–semiconductor field-effect transistor (MOSFETs), several full/semi analytical models have been established by the conformal mapping method [32]–[35]. They were also able to estimate, optimize, and compare the fringe capacitance through simulation results without any fitting parameters.

From a proximity detection model and simulation results with a ring-shaped sensor presented by Chen and Luo [23] and Luo and Chen [26], the solution of cylindrical Laplace's equation was employed and the electric potential distribution from which the fringe capacitance between electrodes bounding the field was calculated. It was found that the dominant parameter in the sensor response is the electrode spacing. Furthermore, it was also stated that the fringe capacitance is proportional to the effective electrode length, defined in this case as the average length of the two electrodes. However, the existing formulations for the fringe field often result in complicated mathematical models from which it is difficult to accurately calculate a given CPS and an extant model can only apply to ideal situations.

Many researches are under their way developing the range of proximity measurement from micrometers to millimeters [36], [37]. To date, the reported target objects for capacitive proximity sensors have been restricted to human finger and metal conductors, with limited distance resolution (below 100mm) [38], [21]. These sensors are mostly based on metal and silicon substrates in a simple printed circuit board (PCB), constituting a number of circuits and complex layered matrix arrays. Other limitations are addressed such as being too brittle to endure large deformation and not flexible enough to cover curved surfaces. Recently, sensor arrays have been made using various polymers such as Parylene, Polyimide (PI), or Polydimethlysiloxane (PDMS) [39]–[41]. These are frequently proposed as the substrates for resistive and capacitive flexible sensors/arrays [18], [22], [12], [42], [43]. Capacitive sensing approaches are less susceptible to temperature variation respected to resistive sensing techniques [22]. However, metal interdigitated electrodes have been designed and fabricated on polymer substrates to implement flexible capacitive micro-sensors [39], [19]. Interfacial adhesion between the metal electrodes, polymer and electrode length on the film were reported to be very challenging [39].

As active sensing elements, nano fillers like Carbon Nanotubes (CNTs) have been the center of attention as an alternative to conventional materials because they have remarkable mechanical/electrical properties [44]–[47]. Particularly, polymers with incorporation of CNTs show great potential with promising features for electronic device platforms. In this regard, vertically aligned CNTs (VACNTs) have been modeled as interdigitated electrodes on a silicon substrate for capacitive sensing [48]. CNTs have also been utilized as the sensing nanofillers for providing conductive polymer composites, which can eliminate the problems of metal film layers patterned on polymer substrates [40]. Different processes have been typically employed to fabricate CNT–polymer nanocomposites sensors, such as mechanical stirring, vacuum filtration, nanoimprint lithography and inkjet printing [47]; however, shaping CNTs in an uniform line pattern as sensing elements are reported to be very complex by these methods [49], [50]. Most of these studies have fabricated planar polymer nanocomposites as strain sensors. Although CNT can provide unique properties to a polymeric structure, it is still a challenge to integrate CNTs within the structure for further applications [51]–[53]. Furthermore, numerous polymer

micromachining processes have been recently developed to implement polymer-based flexible sensors [54], [55].

Therefore, in this article, nanocomposite ultrasensitive proximity sensor exhibits a simple flexible nanostructure compared with previous studies, but with complex microstructure in which CNTs are melt-mixed in the mold substrate thermoplastic polyurethane (TPU). Adding CNTs with different volume rations to the polymer has made continuous variation of the composite electrical conductivity possible which is used to achieve the sensor with controllable sensitivity in this study. The results are made on the basis of a mathematical closed-form model, and a set of experiments corresponding to the mathematical is accomplished to confirm the accuracy of the simulation results. The hypothesis of a fringing electric field sensor is described in our coplanar capacitance sensor in cartesian coordinate. The sensor is designed to be fabricated using flexible polymeric substrate and two thin electrodes located on the both ends. This new design not only simplifies the sensing structure and increases the practical sensing area, but it also offers the opportunity to bring the two electrodes closer or farther together. Calculated and experimental results are presented through the analysis of capacitance behavior and finally voltage distributions of the modeled sensor are simulated over the area between the sensor and the object for different distances and resistivities.

II. FABRICATION AND DESIGN

A. MATERIAL PREPARATION AND SYNTHESIS OF TPU-CNT COMPOSITES

TPU (Elastollan 1185A polyurethane with a density of 1.12g/cm3) and TPU/MWCNT masterbatch (A 5wt% of TPU/MWCNT containing NC7000 MWCNT with 90% purity, a diameter and length of about 9.5 nm and 1.5 μm, respectively) were purchased and diluted. TPU filaments containing 1 and 2 wt % MWCNT were produced by diluting a 5wt % masterbatch of TPU/MWCNT with pure TPU through twin-screw extruder (LabTech Engineering Company LTD., Thailand). The extrusion was performed at 210 °C and 60 rpm. To make TPU-CNT films, pellets were made through cutting TPU-CNT filaments and later compressed in a hot press machine (Carver Inc., Wabash, Indiana) at 2.25 metric tons at 185 °C for 60 seconds. The films were cooled down to the room temperature and utilized to fabricate the sensors and for characterizations. Samples were cut into strips with a size of about 50 × 20 mm squares and a thickness of about 0.5-0.6 mm. (Fig. 1).

B. PROXIMITY MEASURING SYSTEM CONFIGURATIONS

The narrow strip of two ends of samples were coated with CircuitWorks CW2400 conductive silver epoxy to eliminate the noise effects like the penetration depth inside and transverse direction over the film. Tungsten pin probes were then placed on the film ends with a separation of 50 mm and an angle of 45 degree. As shown in figure 1, sensor probes were

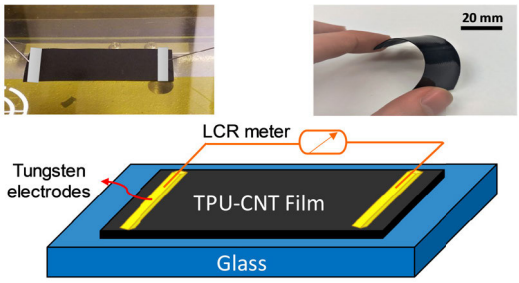

FIGURE 1. Schematic view of the measurement setup and a flexible TPU-CNT film.

mechanically changed to coplanar electrodes due to the silver paste, and technically located on the sensor ends. Capacitance measurements were carried out by using a probing station (Keithley 4200-SCS, Tektronix, USA). Sensing conductive object approached the fixed TPU-CNT film with a constant speed of 6.6 mm/s after 60s waiting time. To detect the maximum change in the capacitance, the samples were presoaked with 5V direct current (DC) to saturate and reduce the tunneling effect. Furthermore, a 30mv alternate current (AC) swiping signal was applied to measure the capacitance of the film with a frequency of 500 kHz to achieve maximum stability of the working window for the fabricated sensors. From the measurements, the value of resistivity of samples varies from 0.1 to 10^5 Ω.m.

III. MATHEMATICAL MODEL

Many capacitive proximity sensing and displacement measurement techniques are built on the use of a field - either electric or magnetic - to detect the presence or position of an object. Technically, an intruding (moving) object performs as a barrier, hindering the electric field and thus reducing the capacitance between electrodes. Thus, this change in capacitance can be reported as the sensitivity of sensor. A schematic view of the proposed sensor together with a moving object and the fringe effect concept were shown in figure 2. As can be seen, two-line electrodes are placed at distance on the polymer-based nanocomposite substrate. When a voltage is applied between the electrodes some amount of current will start flowing inside the substrate resulting in a voltage and charge distribution on the substrate. Moreover, some fringing fields will be developed outside the substrate which contribute on the stored charge on the polymer surface. The current passing to the electrodes is monitored and by dividing the current by the exciting voltage the effective capacitance cam be measured. As an object gets close to the sensor it distorts the fringing fields and consequently changes equivalent(self) C_{eq} and mutual C_m capacitances. These changes in capacitance may be measured and calibrated to measure the distance of the object from the sensor. Figure 3 illustrates a schematic view of the sensor which is composed of two conductive electrodes connected to a polymer substrate. Although the mutual capacitance C_m is increasing by the presence of an object, it is not of a great importance of this study. To measure

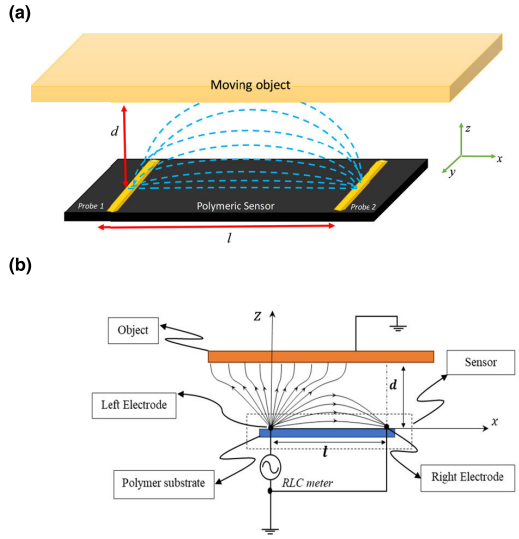

FIGURE 2. Schematic illustration of sensor mechanism for fringe-based TPU-CNT proximity sensor a) 3D model when object is at the farthest distance and not affecting the fringe fields. b) 2D model showing how the fringe field lines are being distracted.

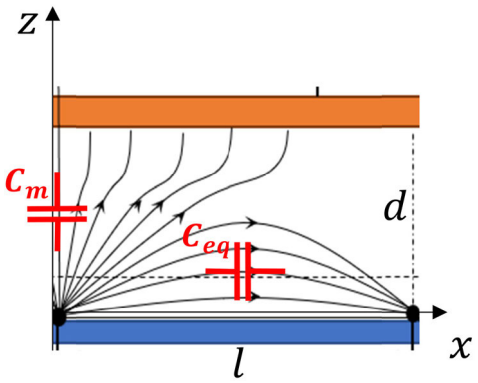

FIGURE 3. Cross section of the rectangular-shaped sensor model with cartesian coordinate system; two different capacitances which specify the sensitivity are shown. C_0 is being measured by LCR meter as a polymer capacitance.

the amount of capacitance between the electrodes (C_{eq}), they are connected to a LCR meter apparatus. When the LCR meter starts to work a sinusoidal voltage of arbitrary frequency is applied between electrodes and therefore opposite charges are stored on them. By definition, the amount of capacitance equals the amplitude of current passing through the LCR meter which stores charges on the electrodes divided by the amplitude of the derivative of the applied voltage with respect to time. It should be noted that only the component of the electrical current which has 90 degrees of difference with the applied voltage should be considered in calculation of the capacitance. That is because due to finite resistivity of the polymer base there will be a component of current which is in phase with the applied voltage, as well.

When the object is far enough from the base polymer substrate, all the lines representing the electric field begin from the left electrode and end in the right one or vice versa. That occurs while as soon as the object which is supposed to be conductive and grounded gets close to the sensor, some electric field lines change their route and will end in the object instead of the electrodes. It is noteworthy that the following solution does not hold for an object with floating potential. In that case, different behavior should be expected and the capacitance increases while the object approaches the sensor and subsequently sensitivity would be proportional to the dielectric constant of the object. Due to this fact as Gauss's law indicate the amount of stored charge on the right-hand side electrode decreases and therefore the measured capacitance declines too. This characteristic of the system may be used to recognize the external object which is approaching the sensor. Experimental measurements show this behavior of the system clearly. In addition to experimental observations, here an analytical analysis of the system will be accomplished with a couple of goals. Firstly an analytical solution helps to higher level of understanding of what happens in the system and secondly quantization of the changes of capacitance with respect to the distance of the object not only helps in calibration of the sensor but also will be beneficial in design of different sensors for various applications.

Due to large dimensions of the system in y -direction, changes of voltage along this axis may be neglected. Therefore, the problem can be modeled as a 2-D one. In what follows we derive the voltage distribution in a rectangular region determined by the following relation:

$$0 \le z \le d, \quad 0 \le x \le l \tag{1}$$

The boundary conditions include:

$$\begin{cases} z = 0 \\ 0 \le x \le l \end{cases} \quad V = V_0(x,t) \quad (a$$

$$\begin{cases} z = d \\ 0 \le x \le l \end{cases} \quad V = 0 \quad (b$$

$$\begin{cases} 0 \le z \le d \\ x = 0 \end{cases} \quad \frac{\partial V}{\partial x} = 0 \quad (c$$

$$\begin{cases} 0 \le z \le d \\ x = l \end{cases} \quad \frac{\partial V}{\partial x} = 0 \quad (d \tag{2}$$

where $V_0(x)$ denotes the voltage distribution on the polymer substrate. Since there is no free stored charge in the part of space enveloped between the polymer substrate and the surface of object, the following equation governs the distribution of voltage in this region:

$$\nabla^2 V(x,y,z,t) = 0 \tag{3}$$

As mentioned above, the problem can be modeled as 2-D, therefore, the above equation turns into:

$$\frac{\partial^2 V(x,z,t)}{\partial x^2} + \frac{\partial^2 V(x,z,t)}{\partial z^2} = 0 \tag{4}$$

According to the boundary conditions given in equation (2), the solution to the above equation can be written as the

following Fourier series:

$$V(x,z,t) = a_0 + b_0 z + \sum_{n=1}^{N} \left(a_n \exp\left(\frac{n\pi z}{l}\right) + b_n \exp\left(-\frac{n\pi z}{l}\right)\right) \cos\left(\frac{n\pi x}{l}\right) \quad (5)$$

In order that the given boundary conditions, be satisfied by the above solution one should have:

$$\sum_{n=1}^{N} (a_n + b_n) \cos\left(\frac{n\pi x}{l}\right) = V_0(x,t) \sum_{n=1}^{N} \left(a_n \exp\left(\frac{n\pi d}{l}\right) + b_n \exp\left(-\frac{n\pi d}{l}\right)\right) \cos\left(\frac{n\pi x}{l}\right) = -a_0 - b_0 d \quad (6)$$

Substituting $z = 0$ and d into equation (5) then integrating both sides with respect to x from 0 to l, results in:

$$a_0 = \frac{1}{l}\int_0^l V_0(x,t)\,dx, \quad b_0 = -\frac{1}{ld}\int_0^l V_0(x,t)\,dx \quad (7)$$

Similarly, multiplying both sides of equation (6) by $\cos\left(\frac{n\pi x}{l}\right)$, then integrating with respect to x from 0 to l, one obtains:

$$a_n + b_n = \frac{2}{l}\int_0^l V_0(x,t)\cos\left(\frac{n\pi x}{l}\right) dx a_n \exp\left(\frac{n\pi d}{l}\right) + b_n \exp\left(-\frac{n\pi d}{l}\right) = 0 \quad (8)$$

Solving the above equation for a_n and b_n, results in:

$$a_n = \frac{2\int_0^l V_0(x,t)\cos\left(\frac{n\pi x}{l}\right)dx}{l\left(1-\exp\left(2\frac{n\pi d}{l}\right)\right)}, \quad b_n = \frac{2\int_0^l V_0(x,t)\cos\left(\frac{n\pi x}{l}\right)dx}{l\left(1-\exp\left(-2\frac{n\pi d}{l}\right)\right)} \quad (9)$$

Therefore, provided that the voltage distribution (V_0) on the polymer substrate is known, its distribution in the region between the polymer substrate and the object surface (V) may be calculated according to equations (5), (7), and (9). Using Gauss's law the charge density per unit length stored on the polymer and object surfaces will be:

$$\lambda_P = -b\varepsilon_0 \left.\frac{\partial V(x,z)}{\partial z}\right|_{z=0} \quad (a$$

$$\lambda_O = b\varepsilon_0 \left.\frac{\partial V(x,z)}{\partial z}\right|_{z=d} \quad (b \quad (10)$$

Additionally, according to law of conservation of charge, one has the following relation governing electrical current I inside the substrate:

$$\frac{dI}{dx} = \frac{d\lambda_P}{dt} \quad (11)$$

Substituting equation (10-a) into equation (11) one obtains:

$$\frac{dI}{dx} = -b\varepsilon_0 \left.\frac{\partial^2 V(x,z,t)}{\partial z \partial t}\right|_{z=0} \quad (12)$$

According to Ohm's law, considering resistance per unit length of the polymer substrate to be represented by ρ, the substrate current may be related to its voltage derivative as:

$$\frac{dV_0}{dx} = \rho I \quad (13)$$

Substituting equation (12) into the above equation, results in:

$$\frac{\partial^2 V_0(x,t)}{\partial x^2} = -\rho b\varepsilon_0 \left.\frac{\partial^2 V(x,z,t)}{\partial z \partial t}\right|_{z=0} \quad (14)$$

Substituting $V(x,z,t)$ from equation (5) into the above equation, one obtains:

$$\frac{\partial^2 V_0(x,t)}{\partial x^2} = -\rho b\varepsilon_0 \left(-\frac{1}{ld}\int_0^l \frac{\partial}{\partial t} V_0(x,t)\,dx + \frac{2\pi}{l^2}\sum_{n=1}^{N} n \left(\begin{array}{l} \frac{\exp\left(2\frac{n\pi d}{l}\right)-\exp\left(-2\frac{n\pi d}{l}\right)}{\left(1-\exp\left(2\frac{n\pi d}{l}\right)\right)\left(1-\exp\left(-2\frac{n\pi d}{l}\right)\right)} \\ \times \int_0^l \frac{\partial}{\partial t} V_0(x,t)\cos\left(\frac{n\pi x}{l}\right)dx \end{array} \right) \times \cos\left(\frac{n\pi x}{l}\right)\right) \quad (15)$$

Multiplying both sides of equation (15) by $\cos\left(\frac{n\pi x}{l}\right)$ when n varies from 0 to N, then integrating with respect to x from 0 to l, one obtains:

$$\left(\frac{\partial V_0(x,t)}{\partial x}\right)\Big|_{x=0}^{l} = -\rho b\varepsilon_0 \left(-\frac{1}{d}\int_0^l \frac{\partial}{\partial t} V_0(x,t)\,dx\right) \quad (16\text{-a})$$

$$\int_0^l \frac{\partial^2 V_0(x,t)}{\partial x^2}\cos\left(\frac{n\pi x}{l}\right)dx = -\rho b\varepsilon_0 \frac{n\pi}{l}\left(\frac{\exp\left(2\frac{n\pi d}{l}\right)-\exp\left(-2\frac{n\pi d}{l}\right)}{\left(1-\exp\left(2\frac{n\pi d}{l}\right)\right)\left(1-\exp\left(-2\frac{n\pi d}{l}\right)\right)} \times \int_0^l \frac{\partial}{\partial t} V_0(x,t)\cos\left(\frac{n\pi x}{l}\right)dx\right) \quad (16\text{-b})$$

Applying the integration by parts method to the left-hand side of equation (16-b), one obtains:

$$\int_0^l \frac{\partial^2 V_0(x,t)}{\partial x^2}\cos\left(\frac{n\pi x}{l}\right)dx = \left(\frac{\partial V_0(x,t)}{\partial x}\cos(n\pi)\right)\Big|_0^l - \left(\frac{n\pi}{l}\right)^2 V_{0n}(t) \quad (17)$$

where:

$$V_{0n}(t) = \int_0^l V_0(x,t)\cos\left(\frac{n\pi x}{l}\right)dx \quad (18)$$

Denoting currents passing through the substrate at $x = 0$ and l, by I_0 and I_l, respectively, according to equation (13) one has:

$$I_0 = \frac{1}{\rho}\left(\frac{\partial V_0(x,t)}{\partial x}\right)\Big|_{x=0}, \quad I_l = \frac{1}{\rho}\left(\frac{\partial V_0(x,t)}{\partial x}\right)\Big|_{x=l} \tag{19}$$

Substituting equations (17), (18) and (19) into (16), results in:

$$I_l - I_0 = \frac{b\varepsilon_0}{d}\dot{V}_{00} \tag{20-a}$$

$$\rho\left(I_l(-1)^n - I_0\right) - \left(\frac{n\pi}{l}\right)^2 V_{0n}(t) = -\rho b\varepsilon_0 \frac{n\pi}{l}\left(\frac{\exp\left(2\frac{n\pi d}{l}\right) - \exp\left(-2\frac{n\pi d}{l}\right)}{\left(1-\exp\left(2\frac{n\pi d}{l}\right)\right)\left(1-\exp\left(-2\frac{n\pi d}{l}\right)\right)}\right)\dot{V}_{0n} \tag{20-b}$$

In the case that the LCR meter applies a sinusoidal voltage of frequency ω to the electrodes, the above equation should be solved with respect to the following boundary conditions:

$$\begin{aligned} x &= 0, \quad V_0 = V_{exc}\cos(\omega t) \\ x &= l, \quad V_0 = 0 \end{aligned} \tag{21}$$

Considering the steady state solutions for of V_0, I_0, and I_l as:

$$\begin{aligned} \tilde{V}_{0n}(t) &= \tilde{v}_{0n}e^{i\omega t} \\ I_0(t) &= i_0 e^{i\omega t} \\ I_l(t) &= i_l e^{i\omega t} \end{aligned} \tag{22}$$

then substituting into equation (20), results in:

$$v_{0n} = \alpha_n i_0 + \beta_n i_l \tag{23}$$

where:

$$\beta_0 = -\alpha_0 = \frac{d}{b\varepsilon_0 i\omega}, \quad \alpha_n = -g(n),$$

$$\beta_n = (-1)^n g(n)\, g(n) = \frac{\rho}{\left[\left(\frac{n\pi}{l}\right)^2 - \rho b\varepsilon_0 \frac{n\pi}{l}\left(\frac{\exp\left(2\frac{n\pi d}{l}\right) - \exp\left(-2\frac{n\pi d}{l}\right)}{\left(1-\exp\left(2\frac{n\pi d}{l}\right)\right)\left(1-\exp\left(-2\frac{n\pi d}{l}\right)\right)}\right) i\omega\right]} \tag{24}$$

$V_0(x,t)$ may be represented using a Fourier series as:

$$V_0(x,t) = \frac{2}{l}\sum_{n=0}^{N} V_{0n}(t)\cos\left(\frac{n\pi x}{l}\right) \tag{25}$$

Substituting equation (25) into (21) results in:

$$\frac{2}{l}\sum_{n=0}^{N} v_{0n} = V_{exc}, \quad \sum_{n=0}^{N} v_{0n}(-1)^n = 0 \tag{26}$$

Using the representation given in equation (23), one has:

$$\left(\sum_{n=0}^{N}\alpha_n\right) i_0 + \left(\sum_{n=0}^{N}\beta_n\right) i_l = \frac{l}{2}V_{exc}\left(\sum_{n=0}^{N}(-1)^n\alpha_n\right) i_0 + \left(\sum_{n=0}^{N}(-1)^n\beta_n\right) i_l = 0 \tag{27}$$

Solving the above equation for i_l, the following expression is found for the input current to the right hand electrode:

$$i_l = \frac{\frac{l}{2}\left(\sum_{n=0}^{N}(-1)^n\alpha_n\right)V_{exc}}{\left(\sum_{n=0}^{N}(-1)^n\alpha_n\right)\left(\sum_{n=0}^{N}\beta_n\right) - \left(\sum_{n=0}^{N}\alpha_n\right)\left(\sum_{n=0}^{N}(-1)^n\beta_n\right)} \tag{28}$$

The total impedance seen by the LCR meter may be calculated through dividing the applied voltage V_{exc} to the input current of the right hand electrode i_l. The real part of derived impedance represents the equivalent resistance due to the finite resistivity of the nanocomposite substrate while its imaginary part represents the equivalent capacitance between the electrodes and the object. Therefore, the following expression may be used for calculation of the equivalent capacitance of the system:

$$C_{eq} = -\frac{Im(i_l)}{\omega V_{exc}}, \quad R_{eq} = -\frac{V_{exc}}{Re(i_l)} \tag{29}$$

IV. RESULTS AND DISCUSSIONS

In this section, analytical closed-form results are discussed and validated by experimental measurements. From the expression model of sensor, equation (29) shows cleraly that the fring capacitance C_{eq} is determined by the geometrical parameters, the proximity distance, relative permittivity, and the resistivity of the sensor design. However, here the geometrical parameters are not of interest to be investigated. Based on the CNT contents inside the film sensor, the resistivity changes from relatively high-resistant sample (the sensor with low volume of CNTs) to very conductive sample containing a great volume of CNTs. From the experimental measurement tests, the value of resistivity for samples varies from 0.1 to $10^5\Omega$.m; yet, by increasing CNTs content, after percolation threshold which takes place in the lower percentage of CNT contents, the resistivity becomes extremely low. So, the TPU with more than 2 wt % CNTs exhibits low resistivity and draws a very high current from LCR meter. Accordingly, in this numerical study the CNT contents are adjusted so that the resistivity falls between 10^2 Ω.m to $10^6\Omega$.m. Frequency 500kHz was earlier experimentally optimized with the purpose of maximize signal to noise ratio (SNR) of measured signals. Fig. 4a. shows the proximity results of the capacitance change for different resistivities of film sensor through the proximity distance of 24cm. The sensor with resistivity of 10^2 Ω.m presents the initial capacitance about 0.045pF at the farthest distance and the capacitance reaches to 0.022pF at the distance of 4cm. As expected by the fringe effect, the capacitance becomes lower in magnitude when the object approaches to the nanocomposite sensor. Furthermore, the analytical model shows that by increasing the resistivity beyond $10^5\Omega$.m, the capacitance is not being affected anymore. While the impedance increases drastically, it demands infinite amount of current which is not feasible. Thus, there

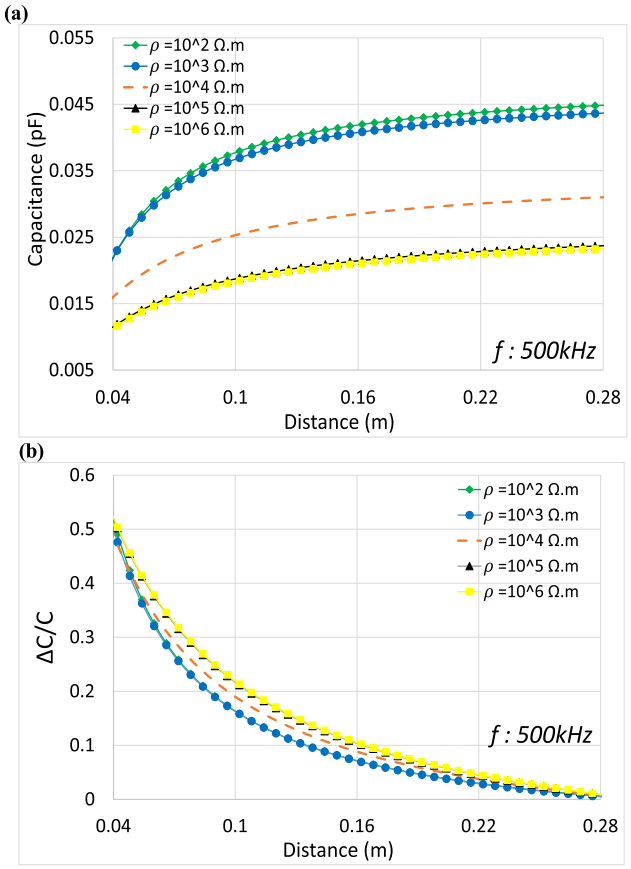

FIGURE 4. Analytically calaculated capacitance versus object proximity for different value of TPU-CNT resistivities at the ecitation frequency of 500kHz a) absolute value b) relative changes.

is no significant effect on the capacitance behavior for the higher resistivity.

To capture the highest sensitivity among different values of resistivity, the absolute change of capacitance to the initial capacitance recorded at the farthest distance (d=28cm) is plotted in figure 4b. Here, the remarkable trend is that the proximity sensitivity of the TPU-CNT sensors rises by increasing the resistivity (lower volume of CNTs). Technically, TPU has been known as a high polar polymer which can be used as a perfect insulator. Addition of CNTs inside the TPU structure, makes the film semi-conductive and increases the effective area of electrodes and consequently the capacitance. Therefore, as evidently expected in fig. 4a, the initial capacitance of the TPU/CNT film has been increased by adding CNTs content. Nevertheless, from fig. 4b, the maximum sensitivity ($\Delta C/C$) is being observed at the lower content of CNTs ($\rho = 105, 106\Omega$.m).

Figs. 5 and 6 show the analytically calculated voltage distribution within the neighboring area between the sensor and object at different values of resistivity. Where, the graph's horizontal axis shows the size of sensor length where electrodes are placed and, the vertical axis indicates the distance with the moving object. Furthermore, contour lines corresponding to certain values of the voltage are plotted together

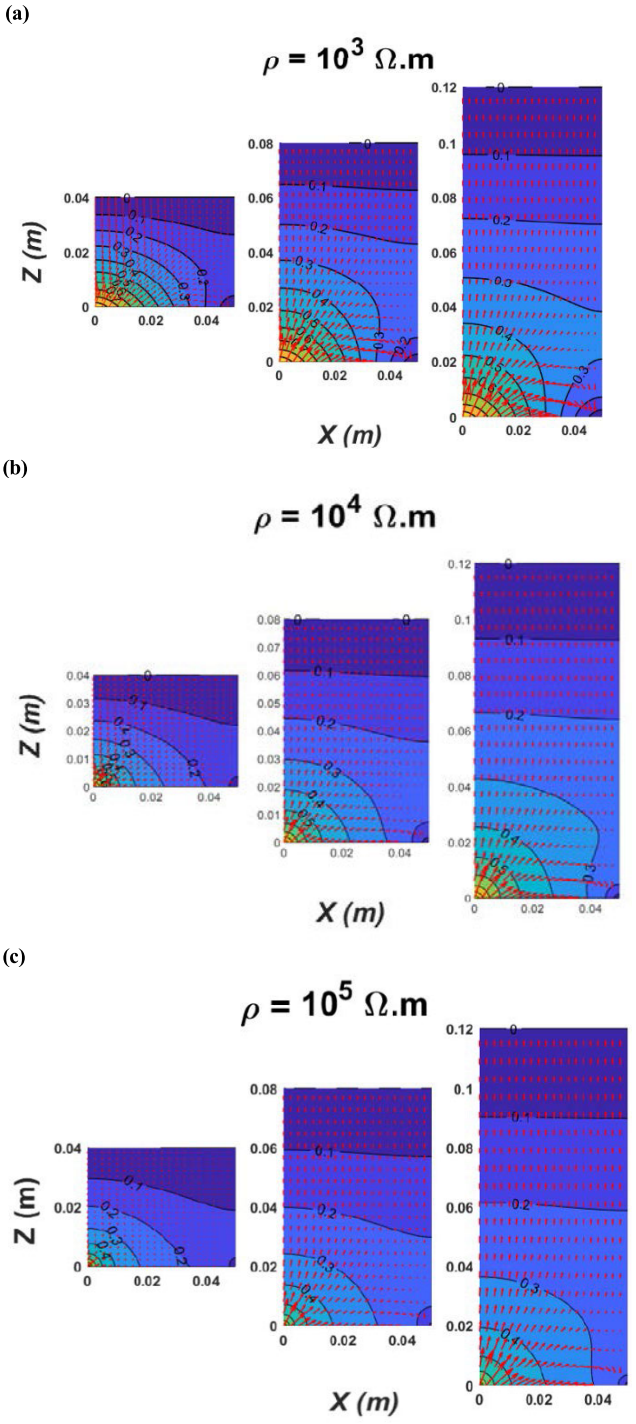

FIGURE 5. Potential contour for the in phase voltages between probes and object for three different location of the object a) $\rho = 10^3\Omega$.m b) $\rho = 10^4\Omega$.m c) $\rho = 10^5\Omega$.m.

with vectors (in red) indicating the magnitude and direction of the electric field at different points. As a consequence of the nonzero electrical resistivity of the sensor both voltage and electric field have some phase difference with respect to the excitation voltage. Therefore, to fully illustrate how these two variables change as functions of time one needs to have both in-phase and out of phase components. These

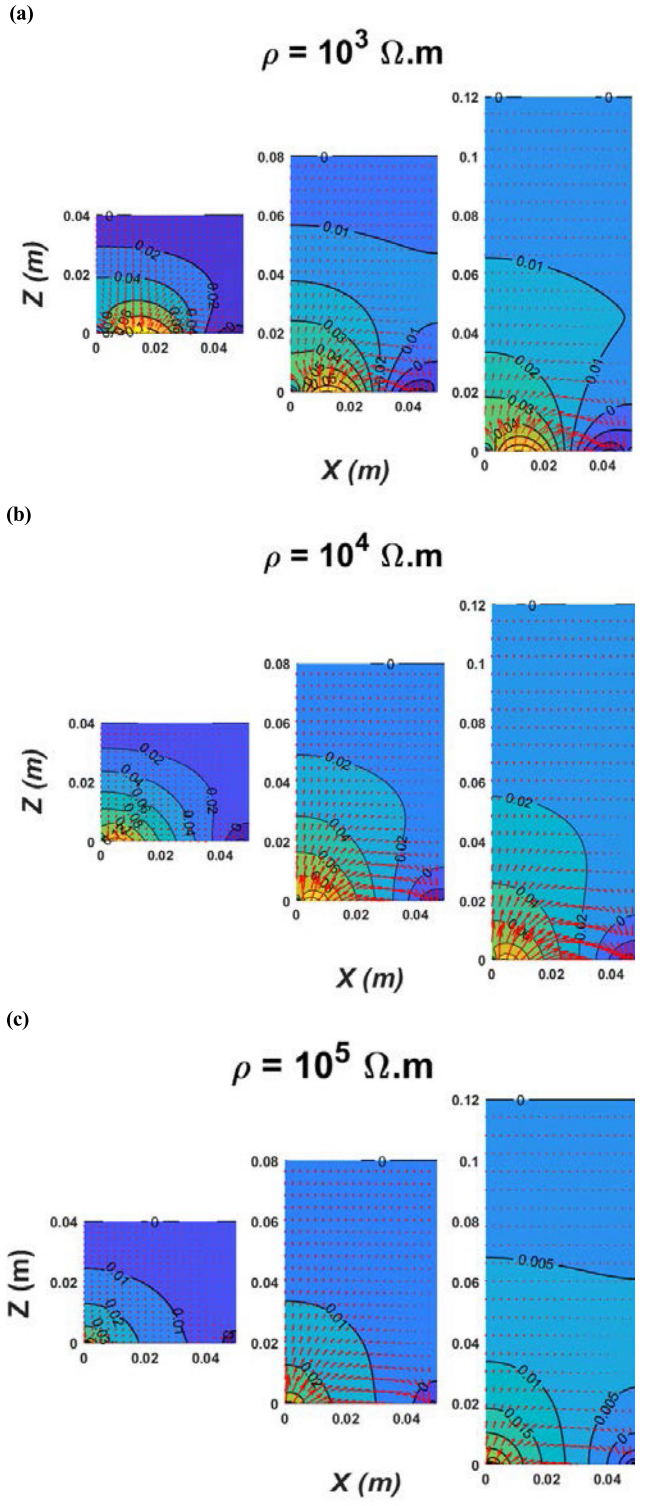

FIGURE 6. Potential contour for the out of phase voltages between probes and object for three different location of the object a) $\rho = 10^3\,\Omega$.m b) $\rho = 10^4\,\Omega$.m c) $\rho = 10^5\,\Omega$.m.

two components are schematically shown in Figs. 5 and 6, respectfully. As seen, when a target object comes closer to the sensor, it interferes with the field lines between the electrodes. As a consequence, the fringing field lines are reconfigured

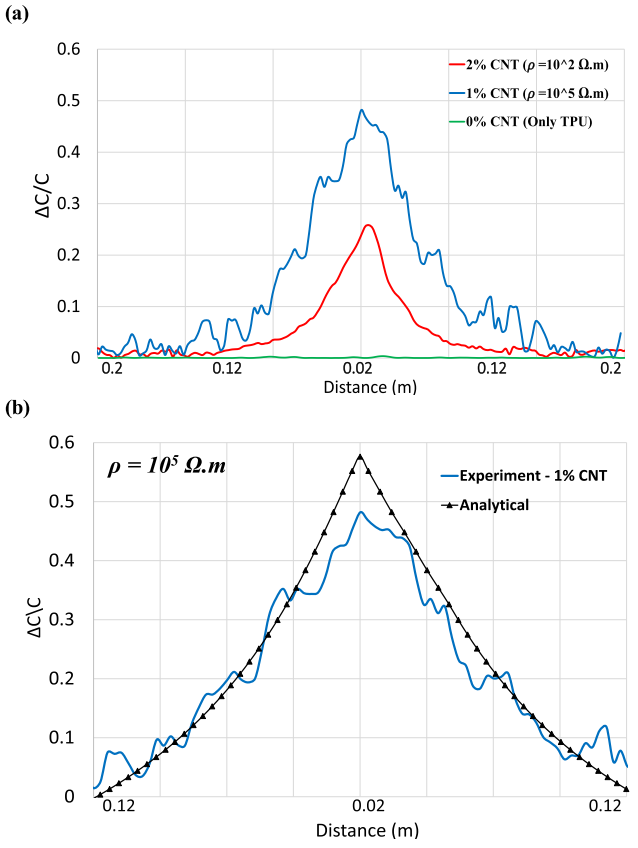

FIGURE 7. Sensitivity (change of capacitance to the initial) comparison (a) empirical sensitivity of different wt %. CNTs through a distance of 0.2 m (b) Simulation result versus experimental one at $\rho = 10^5\,\Omega$.m.

due to presence of the object which in turn reduces the equivalent capacitance (self-capacitance). Additionally, a comparison of the graphs corresponding to different resistivities shows that the electric field at the vicinity of the electrodes is intensified as resistivity decreases. That emerges because at higher conductivities some portion of the stored charge is distributed on the TPU/CNT film leading to enhancement of the effective area of the electrodes, increasing the capacitance, and generating a more intense electric field.

As earlier mentioned, the sensing mechanism is based on the object interference with the electrical field between two probes. The interference disturbed and reduced the number of electric field lines (i.e., C_{eq} self-capacitance) and consequently, stored charges decreased radically over the polymer. To validate that the change of capacitance comes from the fringe phenomenon and also to capture the effect of resistivity, experimental tests are being carried out for three different CNT volumes. Figure 7a. demonstrates that the sensitivity goes up when the film resistivity increases. It closely confirms what the analytical model earlier proved. The experiments also reveal that TPU film containing 1wt% CNTs presents the maximum sensitivity to the proximity sensing. Resistivity of 1wt.% TPU/CNT was earlier measured $10^5\,\Omega$.m. From both analytical and experimental results, it can be deemed that either this CNT volume or a very close volume

would be the optimal nanocomposite sensor out of TPU/CNT, taking into account the sensitivity and impedance.

On the other hand, a comparison of analytical and experimental models is plotted in Fig. 7b over a distance of 0.14m (capacitance variation is being normalized with respect to the initial capacitance). Both plots have shown relatively similar sensitivity behavior and reached to the peak of 0.5-0.6 at the distance of 0.02 m. Apparently, the analytical model results are larger than the measured ones. This discrepancy is primarily introduced by the object used in the measurement. The object dimension was assumed infinite in the analytical model, but finite in the experiment. The body section of the probes is relatively large compared with the size of polymer, which can be other possible sources of error. The difference between the mathematical model and the fabricated nanocomposite sensor is within 10% if the CNT content of polymeric insulator is limited to 1 wt %.

V. CONCLUSION

To summarize, according to the physical cartesian model of fringe capacitances, this article established a 2-D analytical model of the potential, which was based on changing the measured capacitance of rectangular nanocomposite film sensor while an object approached in and moved away. In this work, the modeling of capacitive proximity sensors using the Laplace's equation has proven to be a fast and reliable technique to obtain the capacitance of a capacitive proximity sensor. The resistivity of sensor film demonstrated a significant effect on the sensitivity while it is in the range of 10^3-$10^5\Omega$.m. Accordingly, the fabricated proximity sensor with different volume of CNTs not only clearly confirmed the decreasing trend of the analytical capacitance but it was also compatible with the sensitivity results of the analytical model. As a comparison, 1wt% CNT which its resistivity was measured around $10^5\Omega$.m was plotted over the analytical results with a good agreement. The potential contour of our model has been compared for the different distances from the object, from the probes and for different resistivities.

The calculated capacitance values from the designed tool have been compared to the experimental values and a close agreement between them was observed. This agreement confirmed that the polymeric nano-based sensor as a designed tool can generate optimal capacitive proximity sensitivity in the wide range of detection and accuracy while it has solid-state manufacturing technology.

ACKNOWLEDGMENT

The authors would like to thank Integrated Nanotechnology Development Institute (INDI) for supporting this research. The authors also would like to express their gratitude to the National Science Foundation Major Research Instrumentation Program by supporting this research (Award # 1229514) for the FESEM. Any opinions, findings, and conclusions or recommendations expressed in this material are those of the author(s) and do not necessarily reflect the views of the National Science Foundation.

REFERENCES

[1] J. Park, Y. Lee, J. Hong, Y. Lee, M. Ha, Y. Jung, H. Lim, S. Y. Kim, and H. Ko, "Tactile-direction-sensitive and stretchable electronic skins based on human-skin-inspired interlocked microstructures," *ACS Nano*, vol. 8, no. 12, pp. 12020–12029, Dec. 2014.

[2] S. Tsuji and T. Kohama, "Proximity skin sensor using time-of-flight sensor for human collaborative robot," *IEEE Sensors J.*, vol. 19, no. 14, pp. 5859–5864, Jul. 2019.

[3] I.-J. Cho, H.-K. Lee, S.-I. Chang, and E. Yoon, "Compliant ultrasound proximity sensor for the safe operation of human friendly robots integrated with tactile sensing capability," *J. Electr. Eng. Technol.*, vol. 12, no. 1, pp. 310–316, Jan. 2017.

[4] M. S. Sarwar, Y. Dobashi, C. Preston, J. K. M. Wyss, S. Mirabbasi, and J. D. W. Madden, "Bend, stretch, and touch: Locating a finger on an actively deformed transparent sensor array," *Sci. Adv.*, vol. 3, no. 3, Mar. 2017, Art. no. e1602200.

[5] P. A. Schmidt, E. Maël, and R. P. Würtz, "A sensor for dynamic tactile information with applications in human–robot interaction and object exploration," *Robot. Auto. Syst.*, vol. 54, no. 12, pp. 1005–1014, Dec. 2006.

[6] J. Shin, Z. Liu, W. Bai, Y. Liu, Y. Yan, Y. Xue, I. Kandela, M. Pezhouh, M. R. MacEwan, Y. Huang, W. Z. Ray, W. Zhou, and J. A. Rogers, "Bioresorbable optical sensor systems for monitoring of intracranial pressure and temperature," *Sci. Adv.*, vol. 5, no. 7, Jul. 2019, Art. no. eaaw1899.

[7] A. Atalay, V. Sanchez, O. Atalay, D. M. Vogt, F. Haufe, R. J. Wood, and C. J. Walsh, "Batch fabrication of customizable silicone-textile composite capacitive strain sensors for human motion tracking," *Adv. Mater. Technol.*, vol. 2, no. 9, Sep. 2017, Art. no. 1700136.

[8] H. Guo, X. Pu, J. Chen, Y. Meng, M.-H. Yeh, G. Liu, Q. Tang, B. Chen, D. Liu, S. Qi, C. Wu, C. Hu, J. Wang, and Z. L. Wang, "A highly sensitive, self-powered triboelectric auditory sensor for social robotics and hearing aids," *Sci. Robot.*, vol. 3, no. 20, Jul. 2018, Art. no. eaat2516.

[9] Y. Wu, Y. Liu, Y. Zhou, Q. Man, C. Hu, W. Asghar, F. Li, Z. Yu, J. Shang, G. Liu, and M. Liao, "A skin-inspired tactile sensor for smart prosthetics," *Sci. Robot.*, vol. 3, no. 22, 2018, Art. no. eaat0429.

[10] W. Gao, S. Emaminejad, H. Y. Y. Nyein, S. Challa, K. Chen, A. Peck, H. M. Fahad, H. Ota, H. Shiraki, D. Kiriya, D.-H. Lien, G. A. Brooks, R. W. Davis, and A. Javey, "Fully integrated wearable sensor arrays for multiplexed in situ perspiration analysis," *Nature*, vol. 529, no. 7587, pp. 509–514, 2016.

[11] B.-C. Zhang, H. Wang, Y. Zhao, F. Li, X.-M. Ou, B.-Q. Sun, and X.-H. Zhang, "Large-scale assembly of highly sensitive Si-based flexible strain sensors for human motion monitoring," *Nanoscale*, vol. 8, no. 4, pp. 2123–2128, 2016.

[12] C.-L. Choong, M.-B. Shim, B.-S. Lee, S. Jeon, D.-S. Ko, T.-H. Kang, J. Bae, S. H. Lee, K.-E. Byun, J. Im, Y. J. Jeong, C. E. Park, J.-J. Park, and U.-I. Chung, "Highly stretchable resistive pressure sensors using a conductive elastomeric composite on a micropyramid array," *Adv. Mater.*, vol. 26, no. 21, pp. 3451–3458, Jun. 2014.

[13] S. Y. Kim, S. Park, H. W. Park, D. H. Park, Y. Jeong, and D. H. Kim, "Highly sensitive and multimodal all-carbon skin sensors capable of simultaneously detecting tactile and biological stimuli," *Adv. Mater.*, vol. 27, no. 28, pp. 4178–4185, 2015.

[14] S. Harada, K. Kanao, Y. Yamamoto, T. Arie, S. Akita, and K. Takei, "Fully printed flexible fingerprint-like three-axis tactile and slip force and temperature sensors for artificial skin," *ACS Nano*, vol. 8, no. 12, pp. 12851–12857, Dec. 2014.

[15] M. R. Kulkarni, R. A. John, M. Rajput, N. Tiwari, N. Yantara, A. C. Nguyen, and N. Mathews, "Transparent flexible multifunctional nanostructured architectures for non-optical readout, proximity, and pressure sensing," *ACS Appl. Mater. Interface*, vol. 9, no. 17, pp. 15015–15021, May 2017.

[16] T. Kohama and S. Tsuji, "Tactile and proximity measurement by 3D tactile sensor using self-capacitance measurement," in *Proc. IEEE SENSORS*, Nov. 2015, pp. 1–4.

[17] O. O. Ojuroye, R. N. Torah, A. O. Komolafe, and S. P. Beeby, "Embedded capacitive proximity and touch sensing flexible circuit system for electronic textile and wearable systems," *IEEE Sensors J.*, vol. 19, no. 16, pp. 6975–6985, Aug. 2019.

[18] B. Zhang, Z. Xiang, S. Zhu, Q. Hu, Y. Cao, J. Zhong, Q. Zhong, B. Wang, Y. Fang, B. Hu, J. Zhou, and Z. Wang, "Dual functional transparent film for proximity and pressure sensing," *Nano Res.*, vol. 7, no. 10, pp. 1488–1496, Oct. 2014.

[19] R. Matsuzaki and A. Todoroki, "Wireless flexible capacitive sensor based on ultra-flexible epoxy resin for strain measurement of automobile tires," *Sens. Actuators A, Phys.*, vol. 140, no. 1, pp. 32–42, Oct. 2007.
[20] K. Koibuchi, K. Saw, T. Honma, T. Hayashi, K. Ueda, and H. Sasaki, "Loss estimation and sensing property enhancement for eddy-current-type proximity sensor," *IEEE Trans. Magn.*, vol. 42, no. 4, pp. 1447–1450, Apr. 2006.
[21] G. Langfelder, A. F. Longoni, A. Tocchio, and E. Lasalandra, "MEMS motion sensors based on the variations of the fringe capacitances," *IEEE Sensors J.*, vol. 11, no. 4, pp. 1069–1077, Apr. 2011.
[22] H.-K. Lee, S.-I. Chang, and E. Yoon, "Dual-mode capacitive proximity sensor for robot application: Implementation of tactile and proximity sensing capability on a single polymer platform using shared electrodes," *IEEE Sensors J.*, vol. 9, no. 12, pp. 1748–1755, Dec. 2009.
[23] Z. Chen and R. C. Luo, "Design and implementation of capacitive proximity sensor using microelectromechanical systems technology," *IEEE Trans. Ind. Electron.*, vol. 45, no. 6, pp. 886–894, Dec. 1998.
[24] X. Hu and W. Yang, "Planar capacitive sensors—Designs and applications," *Sensor Rev.*, vol. 30, no. 1, pp. 24–39, Jan. 2010.
[25] T. Sivayogan, "Design and development of a contactless planar capacitive sensor," M.S. thesis, Univ. Toronto, Toronto, ON, Canada, 2013.
[26] R. C. Luo and Z. Chen, "Modeling and implementation of an innovative micro proximity sensor using micromachining technology," in *Proc. IEEE/RSJ Int. Conf. Intell. Robots Syst. (IROS)*, Jul. 1993, pp. 1709–1716.
[27] R. C. Joy and E. S. Schlig, "Thermal properties of very fast transistors," *IEEE Trans. Electron Devices*, vol. 17, no. 8, pp. 586–594, Aug. 1970.
[28] J. L. Novak and J. J. Wiczer, "A high resolution capacitive imaging sensor for manufacturing applications," Sandia Nat. Labs., Albuquerque, NM, USA, Tech. Rep. 6232496, 1990. [Online]. Available: https://www.osti.gov/biblio/6232496
[29] B. Noltingk, N. Be, and N. Aet, "Theory and application of a proximity gauge using fringing capacitance," in *Proc. ACTA IMEKO*, 1976, pp. 537–549.
[30] W.-C. Chuang, C.-W. Wang, W.-C. Chu, P.-Z. Chang, and Y.-C. Hu, "The fringe capacitance formula of microstructures," *J. Micromech. Microeng.*, vol. 22, no. 2, Feb. 2012, Art. no. 025015.
[31] R. H. Bhuiyan, R. A. Dougal, and M. Ali, "Proximity coupled interdigitated sensors to detect insulation damage in power system cables," *IEEE Sensors J.*, vol. 7, no. 12, pp. 1589–1596, Dec. 2007.
[32] Y. Sun, Z. Liu, X. Li, J. Ren, F. Zheng, and Y. Shi, "Analytical gate fringe capacitance model for nanoscale MOSFET with layout dependent effect and process variations," *J. Phys. D, Appl. Phys.*, vol. 51, no. 27, Jul. 2018, Art. no. 275104.
[33] A. Bansal, B. C. Paul, and K. Roy, "Modeling and optimization of fringe capacitance of nanoscale DGMOS devices," *IEEE Trans. Electron Devices*, vol. 52, no. 2, pp. 256–262, Feb. 2005.
[34] X. Liu, X. Jin, J.-H. Lee, L. Zhu, H.-I. Kwon, and J.-H. Lee, "A full analytical model of fringing-field-induced parasitic capacitance for nanoscaled MOSFETs," *Semicond. Sci. Technol.*, vol. 25, no. 1, Jan. 2010, Art. no. 015008.
[35] M. Wang, D.-M. Ke, C.-X. Xu, and B.-T. Wang, "A 2-D semi-analytical model of parasitic capacitances for MOSFETs with high K gate dielectric in short channel," *Solid-State Electron.*, vol. 92, pp. 35–39, Feb. 2014.
[36] D.-C. Wang, J.-C. Chou, S.-M. Wang, P.-L. Lu, and L.-P. Liao, "Application of a fringe capacitive sensor to small-distance measurement," *Jpn. J. Appl. Phys.*, vol. 42, p. 5816, Sep. 2003.
[37] C.-F. Hu, W.-S. Su, and W. Fang, "Development of patterned carbon nanotubes on a 3D polymer substrate for the flexible tactile sensor application," *J. Micromech. Microeng.*, vol. 21, no. 11, Nov. 2011, Art. no. 115012.
[38] M. Kang, J. Kim, B. Jang, Y. Chae, J.-H. Kim, and J.-H. Ahn, "Graphene-based three-dimensional capacitive touch sensor for wearable electronics," *ACS Nano*, vol. 11, no. 8, pp. 7950–7957, Aug. 2017.
[39] C.-Y. Lee, G.-W. Wu, and W.-J. Hsieh, "Fabrication of micro sensors on a flexible substrate," *Sens. Actuators A, Phys.*, vol. 147, no. 1, pp. 173–176, Sep. 2008.
[40] C.-X. Liu and J.-W. Choi, "Patterning conductive PDMS nanocomposite in an elastomer using microcontact printing," *J. Micromech. Microeng.*, vol. 19, no. 8, Aug. 2009, Art. no. 085019.
[41] S. Khan, S. Tinku, L. Lorenzelli, and R. S. Dahiya, "Flexible tactile sensors using screen-printed P(VDF-TrFE) and MWCNT/PDMS composites," *IEEE Sensors J.*, vol. 15, no. 6, pp. 3146–3155, Jun. 2015.
[42] L. Pan, A. Chortos, G. Yu, Y. Wang, S. Isaacson, R. Allen, Y. Shi, R. Dauskardt, and Z. Bao, "An ultra-sensitive resistive pressure sensor based on hollow-sphere microstructure induced elasticity in conducting polymer film," *Nature Commun.*, vol. 5, no. 1, p. 3002, May 2014.
[43] H. Vandeparre, D. Watson, and S. P. Lacour, "Extremely robust and conformable capacitive pressure sensors based on flexible polyurethane foams and stretchable metallization," *Appl. Phys. Lett.*, vol. 103, no. 20, Nov. 2013, Art. no. 204103.
[44] E. B. Secor and M. C. Hersam, "Emerging carbon and post-carbon nanomaterial inks for printed electronics," *J. Phys. Chem. Lett.*, vol. 6, no. 4, pp. 620–626, Feb. 2015.
[45] K. Arapov, E. Rubingh, R. Abbel, J. Laven, G. de With, and H. Friedrich, "Conductive screen printing inks by gelation of graphene dispersions," *Adv. Funct. Mater.*, vol. 26, no. 4, pp. 586–593, Jan. 2016.
[46] I. A. Kinloch, J. Suhr, J. Lou, R. J. Young, and P. M. Ajayan, "Composites with carbon nanotubes and graphene: An outlook," *Science*, vol. 362, no. 6414, pp. 547–553, Nov. 2018.
[47] S. Khan, L. Lorenzelli, and R. S. Dahiya, "Technologies for printing sensors and electronics over large flexible substrates: A review," *IEEE Sensors J.*, vol. 15, no. 6, pp. 3164–3185, Jun. 2015.
[48] Y. Abdi, A. Ebrahimi, S. Mohajerzadeh, and M. Fathipour, "High sensitivity interdigited capacitive sensors using branched treelike carbon nanotubes on silicon membranes," *Appl. Phys. Lett.*, vol. 94, no. 17, Apr. 2009, Art. no. 173507.
[49] N. Hu, Y. Karube, M. Arai, T. Watanabe, C. Yan, Y. Li, Y. Liu, and H. Fukunaga, "Investigation on sensitivity of a polymer/carbon nanotube composite strain sensor," *Carbon*, vol. 48, no. 3, pp. 680–687, Mar. 2010.
[50] J. Kettle, S. Whitelegg, A. M. Song, D. C. Wedge, L. Kotacka, V. Kolarik, M. B. Madec, S. G. Yeates, and M. L. Turner, "Fabrication of planar organic nanotransistors using low temperature thermal nanoimprint lithography for chemical sensor applications," *Nanotechnology*, vol. 21, no. 7, Feb. 2010, Art. no. 075301.
[51] X. Song, S. Liu, Z. Gan, Q. Lv, H. Cao, and H. Yan, "Controllable fabrication of carbon nanotube-polymer hybrid thin film for strain sensing," *Microelectron. Eng.*, vol. 86, no. 11, pp. 2330–2333, Nov. 2009.
[52] W.-S. Su, C.-M. Lin, T.-H. Chen, and W. Fang, "Patterning and growth of carbon nanotubes on a highly structured 3D substrate surface," *J. Micromech. Microeng.*, vol. 19, no. 10, Oct. 2009, Art. no. 105009.
[53] H. Shen, J. Qiu, and M. Balsi, "Vibration damping as a result of piezoelectric energy harvesting," *Sens. Actuators A, Phys.*, vol. 169, no. 1, pp. 178–186, 2011.
[54] W. Tang, M. H. Santare, and S. G. Advani, "Melt processing and mechanical property characterization of multi-walled carbon nanotube/high density polyethylene (MWNT/HDPE) composite films," *Carbon*, vol. 41, no. 14, pp. 2779–2785, 2003.
[55] Z. Spitalsky, D. Tasis, K. Papagelis, and C. Galiotis, "Carbon nanotube-polymer composites: Chemistry, processing, mechanical and electrical properties," *Prog. Polym. Sci.*, vol. 35, pp. 357–401, 2010.

REZA MOHEIMANI received the M.S. degree in mechanical engineering from the Sharif University of Technology, in 2012, and the second master's degree in material science and engineering from Washington State University, in 2017. He is currently pursuing the Ph.D. degree with Purdue University. His research interests include thermomechanical characterization of composite structures and nanopolymeric capacitive sensors.

ABDOLREZA PASHARAVESH received the two B.S. degrees in electrical and mechanical engineering from the Sharif University of Technology, Iran, in 2009, where he is currently pursuing the master's and Ph.D. degrees in mechanical engineering. He is a Research Associate with Purdue University. He is also teaching mechatronic, control, and nonlinear vibration.

MANGILAL AGARWAL (Senior Member, IEEE) received the Ph.D. degree in engineering (micro/nanotechnology concentration) from Louisiana Tech University, in 2004. He is currently the Director of the Integrated Nanosystems Development Institute (INDI), Purdue School of Engineering and Technology, IUPUI, Indianapolis, IN, USA. He has more than 20 years of experience in nano materials. His primary research interest includes design and development of nanosensors that can smell using a canine-inspired model. He also investigates the design/fabrication of flexible energy devices and systems.

HAMID DALIR (Senior Member, IEEE) received the Ph.D. degree in mechanical engineering from the Tokyo Institute of Technology, in September 2009. He was the Technical Director of the Syracuse Center of Excellence for Analysis and Design, Department of Mechanical and Aerospace Engineering, Syracuse University, from 2015 to 2017. He is currently the Director of the Advanced Composite Structures Engineering Laboratory (ACSEL), Purdue School of Engineering and Technology, IUPUI, Indianapolis, IN, USA. His primary research interests include the general area of solid mechanics and specifically on stress, modal, and thermal analysis of mechanical and aerospace structures. He is a Senior Member of AIAA, ASME, and ASC.